

On the ferromagnetic character of $(\text{LaVO}_3)_m/\text{SrVO}_3$ superlattices

Cosima Schuster,¹ Ulrike Lüders,² Udo Schwingenschlögl,³ and Raymond Frésard²

¹*Universität Augsburg, Institut für Physik, 86135 Augsburg, Germany*

²*Laboratoire CRISMAT, UMR CNRS-ENSICAEN 6508, 14050 Caen, France*

³*KAUST, PSE Division, Thuwal 23955-6900, Kingdom of Saudi Arabia*

The experimental observation that vanadate superlattices $(\text{LaVO}_3)_m/\text{SrVO}_3$ show ferromagnetism up to room temperature [U. Lüders *et al.*, Phys. Rev. B **80**, 241102R (2009)] is investigated by means of density functional theory. First, the influence of the density functional on the electronic and magnetic structure of bulk LaVO_3 is discussed. Second, the band structure of a $(\text{LaVO}_3)_m/\text{SrVO}_3$ slab for $m = 5$ and 6 is calculated. Very different behaviors for odd and even values of m are found: In the odd case lattice relaxation results into a buckling of the interface VO_2 layers that leads to spin-polarized interfaces. In the even case a decoupling of the interface VO_2 layers from the LaO layers is obtained, confining the interface electrons into a two-dimensional electron gas. The orbital reconstruction at the interface due to the lattice relaxation is discussed.

PACS numbers: 71.15.Mb, 73.21.Cd, 75.70.Cn

Keywords: Electronic structure calculation, superlattice, ferromagnetism in reduced dimensions

I. INTRODUCTION

The combination of low dimensionality and strong correlations proved fruitful in the quest for new materials with functional-oriented properties. It led to the high- T_c superconductivity,^{1,2} transparent conducting oxides,³ high capacitance heterostructures,⁴ and large thermopower,⁵ to quote a few. Recently, the creation of high-mobility electron gases with reduced dimensionality has also been pursued in artificially layered oxide systems. They include (i) the interface between the two insulators SrTiO_3 and LaAlO_3 ,⁶⁻⁸ (ii) systems with ultra-thin doping layers as $\text{Nb}:\text{SrTiO}_3$ in SrTiO_3 ,⁹ and RO layers with $\text{R} = \text{La}, \text{Pr}, \text{Nd}$ in SrTiO_3 ,¹⁰ and (iii) the surface of SrTiO_3 .¹¹ In some of these systems functional properties were found, such as superconductivity¹² and ferromagnetism.¹³

Charge carriers with reduced dimensionality can be introduced in other complex oxides, too. For instance, ultra-thin SrVO_3 layers can be intercalated in LaVO_3 ,¹⁴ resulting in ferromagnetism up to room temperature¹⁵ although none of the two oxides is magnetic at this temperature. This points out the relevance of the layered geometry, since the solid solution $\text{La}_{1-x}\text{Sr}_x\text{VO}_3$ shows the typical phase diagram of a doped Mott-insulator with a transition from an antiferromagnetic insulator to a non-magnetic metal at about $x = 0.2$.^{16,17} Contrary to the solid solution, $(\text{LaVO}_3)_m/\text{SrVO}_3$ superlattices show ferromagnetic behavior above room temperature for m ranging from 3 to 6, with a higher magnetization for even m values than for odd values. Thus, the geometrically confined doping in the superlattices gives rise to a magnetic phase which is not observed in the randomly doped solid solution.

From the theoretical point of view, the reduced dimension of electronic states confined in a potential created by the interface of two insulators, or by geometrically confined doping, leads to a renewed interest in two-dimensional systems. Studies of the three band Hubbard

model predict a ferromagnetic ground state in case of $2/3$ and $3/4$ band filling for a reduced bandwidth due to the enhanced correlations of the electrons.¹⁸ Ferromagnetism was also theoretically predicted for a model specific to two t_{2g} orbitals,¹⁹ at $\text{SrTiO}_3/\text{LaVO}_3$ interfaces²⁰ and in $\text{SrTiO}_3/\text{SrVO}_3$ superlattices,²¹ indicating a strong coupling of the electronic, magnetic and orbital degrees of freedom to the geometry of the superlattice including the number of SrVO_3 layers. Again, in both cases the magnetic phase was largely explained by the confinement and a change in the orbital occupations.

However, in the case of superlattices or heterostructures, the reduced bandwidth and therefore enhanced correlations are just one part of the story. As in those systems two different materials are epitaxially grown on top of each other, also the misfit of the lattice parameters of both materials plays a role for the properties of the system mediated by the distortion of the structure due to strain. Especially in oxides the distortion can have a strong influence on the properties since, as mentioned above, the electronic, spin and lattice degrees of freedom are strongly coupled. This effect was shown theoretically in distorted LaVO_3 where, depending on the distortion of the lattice, different antiferromagnetic structures become energetically favorable.²²

In order to analyze the ferromagnetic state observed in $(\text{LaVO}_3)_m/\text{SrVO}_3$ superlattices, electronic band structure calculations are helpful to confirm the confinement of the electronic states and to elucidate the origin of the ferromagnetism. For this purpose, we will use density functional theory and address the distortion of the lattice. Furthermore, the superlattices show an asymmetry of the magnetic properties between odd and even numbers of LaVO_3 unit cells. Thus, one aim of the calculations is to provide evidences for a possible difference in confinement between the two geometries.

The paper is organized as follows. In Sec. II we discuss the influence of the density functional on the electronic and magnetic structure of bulk LaVO_3 . The structure

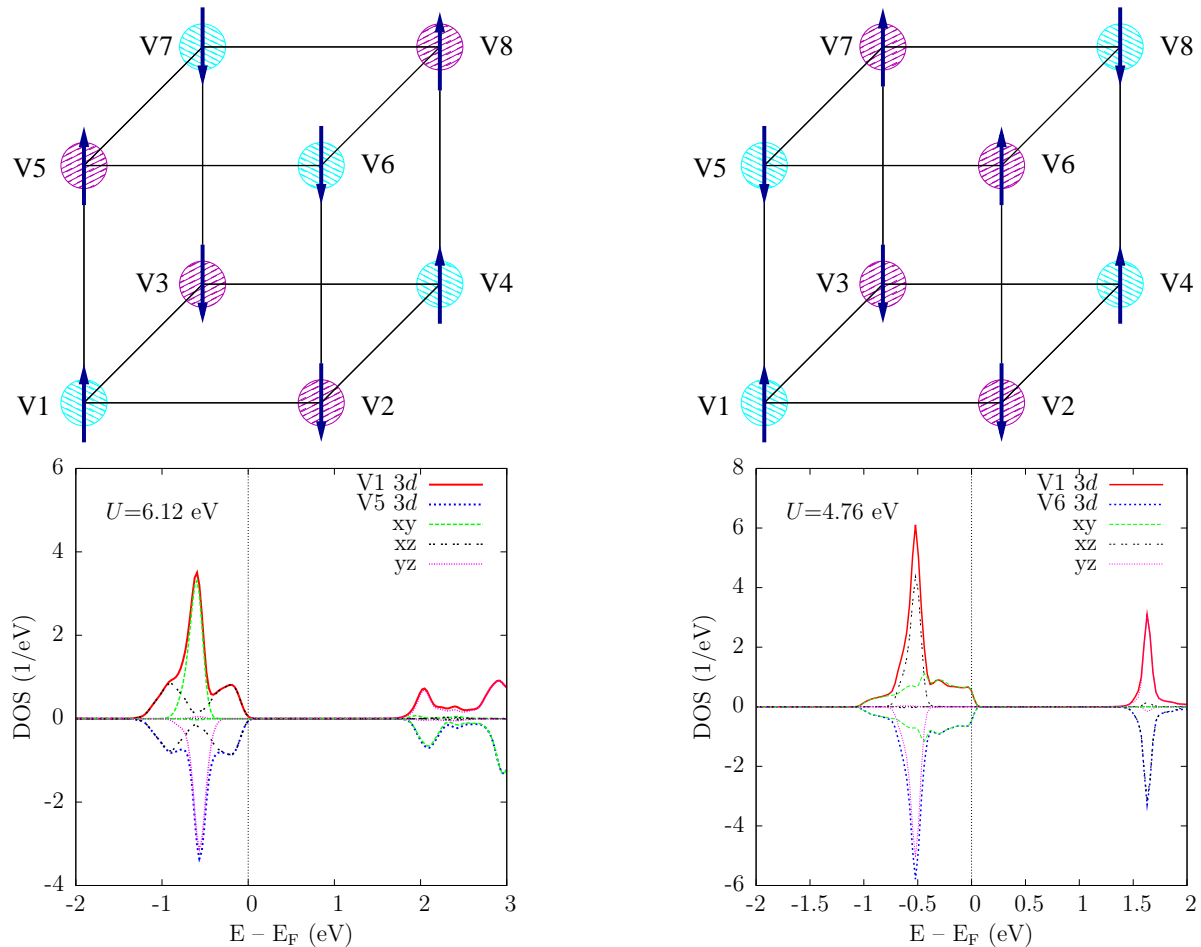


FIG. 1: (Color online) Top: Proposed spin and orbital order in the rare earth vanadates. Bottom: Density of states projected on the V $3d$ orbitals. Left: C-type spin ordered LaVO_3 . Right: G-type spin ordered LaVO_3 . The orbital occupancy of the V1 atom in the left lower corner (red line) is compared to the orbital occupancy of the according V of the upper layer with the same spin orientation (blue line). The latter DOS is multiplied by -1 and plotted along the negative y -axis. The c/a ratio is 1.02.

model of $(\text{LaVO}_3)_m/\text{SrVO}_3$ superlattices is addressed in Sec. III, followed by the electronic structure, the charge carrier distribution and the orbital occupancy of the $m = 5$ and $m = 6$ superlattices, as representative of even and odd superlattices, respectively. Finally, our findings are summarized in Sec. IV.

II. ELECTRONIC AND MAGNETIC STRUCTURE OF BULK LaVO_3

There are many systems for which there is a consensus about the appropriate density functional. This is not the case for the vanadates and we therefore start our considerations addressing this point. The rare earth vanadates with perovskite structure, including LaVO_3 , have the V ion in a $3+$ valence state, i.e., the two electrons in the V $3d$ shell occupy two of the t_{2g} orbitals with $S = 1$.

The crystal field splitting of the $3d$ orbitals in threefold degenerate t_{2g} and twofold degenerate e_g orbitals is a consequence of the octahedral coordination of the V ions by O atoms. The rare earth vanadates show simultaneous antiferro-type spin and orbital ordering.²⁴ The spin ordering of LaVO_3 is C-type, i.e., the alignment is antiferromagnetic within the xy -plane and ferromagnetic along the z -direction.²³ The accompanying orbital order is G-type, i.e., it alternates in all directions. Other vanadates show G-type spin ordering together with C-type orbital ordering. For an overview of the phase diagram see Ref. 24. It has been shown in Ref. 22 that strain due to the coherent growth on a substrate can strongly affect the orbital ordering. For an increasing c/a ratio the G-type order is destabilized.

It is essential that the approximation to the density functional treats the lattice, magnetic, and electronic properties on an equal level. While the local density

approximation (LDA) typically underestimates the bond lengths and magnetic couplings, the generalized gradient approximation (GGA) overestimates both. For bulk LaVO_3 , the GGA correctly predicts the C-type spin ordering, while the LDA tends to delocalize the electronic states, which is critical in the case of narrow $3d$ bands. To obtain an insulating state, corrections beyond the LDA/GGA have to be considered, such as the LDA/GGA+ U approach in which a local interaction is added for the $3d$ orbitals.²⁵ This enhances the separation of the $3d$ energy levels and opens a band gap. It is found that the magnetic ordering can be changed by this treatment.²⁶

A further step towards a rigorous treatment can be achieved by hybrid functionals which incorporate a non-local Fock exchange. Hybrid functionals such as PBE0 and HSE yield an electronic structure comparable to self-consistent GW calculations for much lower computational cost. Even the local EECCE approach has shown clear advantages over the LDA/GGA+ U in describing the electronic structure in nickelate stripe phases.²⁷ However, it is known that the Fock term (without correction of the correlation term) results in a substantial overestimation of the magnetic coupling and, therefore, in an unreliable determination of the magnetic ordering, including phase transitions. A GW treatment leads to accurate electronic structures and magnetic phase transitions but is computationally too costly for superlattice systems. The best compromise therefore is the LDA/GGA+ U approach, which we apply in the following. Specifically, we employ the WIEN2k augmented plane wave plus local orbitals code.²⁸ We find that the energies and electronic states obtained for the fully localized and around mean field double counting corrections show the same behavior.

The interaction parameter U is adjusted as follows. For $U > 5$ eV the C-type spin ordering is energetically favored over the G-type ordering. A band gap of 1.5 eV is obtained for $U = 6.12$ eV in the case of C-type spin ordering, while the same gap is found in the case of G-type spin ordering for $U = 4.8$ eV, see Fig. 1. In addition, the C-type orbital ordering under G-type spin ordering depends only weakly on U and on the lattice strain. On the other hand, the G-type orbital ordering under C-type spin ordering is very sensitive to strain. Disorder or ferro-type orbital ordering is found for $c/a > 1$ (which is fulfilled in our superlattice system). Ferromagnetism and A-type antiferromagnetism result in higher energies than the C- and G-type spin orderings for all approximations under study. Electronic densities of states for C-type and G-type spin ordered LaVO_3 for $c/a = 1.02$ are shown in Fig. 1. While the G-type density of states (DOS) indicates very narrow bands, the bands are much broader for C-type spin ordering despite the higher U value. For C-type spin ordering, the d_{xz} orbital, forming a double peak, is occupied, while the $d_{xy/yz}$ orbitals are partially occupied and therefore subject to orbital ordering, in agreement with Ref. 22. In contrast, for G-type spin ordering, the d_{xy} orbital is occupied, with a much

less pronounced DOS structure, and the orbital ordering affects the $d_{xz/yz}$ orbitals.

Within GGA the ground state of bulk SrVO_3 is antiferromagnetic with $\mu_V = 0.2 \mu_B$, but the energy difference to the non-magnetic solution is small, amounting to 0.2 meV per V atom.²⁹ For the GGA+ U method, the C-type antiferromagnet is favored by 30 meV per V atom over the A-type antiferromagnet and by 140 meV per V atom over the ferromagnet. A local hybrid approach with 25% Fock mixing would favor G-type spin ordering, since a C-type starting configuration changes to G-type during the self-consistency calculation. The onsite interaction does not open a band gap in bulk SrVO_3 but the compound stays metallic. Around the Fermi energy, we find the t_{2g} orbitals equally partially occupied, while the e_g orbitals are empty. Even though the spin-orbit coupling has little impact on the ground state of LaVO_3 it must be included in the case of SrVO_3 .²¹ Indeed it splits the t_{2g} states and gives rise to a band gap of 0.61 eV. In this case C-type spin ordering (magnetization in the x -direction) comes along with filled d_{xy} and half-filled $d_{xz,yz}$ orbitals, yielding ferro-type orbital ordering.

III. $(\text{LaVO}_3)_m/(\text{SrVO}_3)$ SUPERLATTICES

The structure setup for the calculations of the superlattice starts from the tetragonal phase of LaVO_3 , neglecting an orthorhombic lowering of the symmetry due to rotations of the oxygen octahedra. In addition, ideal atomically sharp interfaces are studied. We put one SrVO_3 layer between $m = 5$ or $m = 6$ LaVO_3 layers, representa-

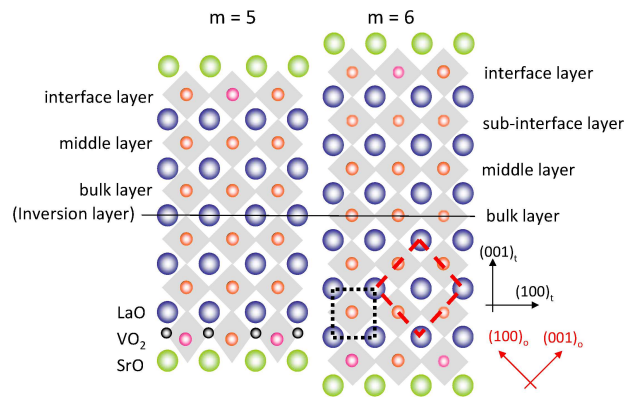


FIG. 2: (Color online) Supercell setup for the $(\text{LaVO}_3)_m/\text{SrVO}_3$ heterostructure for $m = 5$ (left) and $m = 6$ (right). La (Sr) atoms are represented by blue (green) spheres and V^{3+} (V^{2+}) ions are represented by orange (pink) spheres. The grey squares indicate the oxygen octahedra. The oxygen atoms themselves are omitted, except for the bottom interface layer for $m = 5$ where black spheres are shown to highlight the buckling of the VO_2 layer. In the bottom of the $m = 6$ structure the (101) plane of the tetragonal (orthorhombic) cell is indicated in black (red).

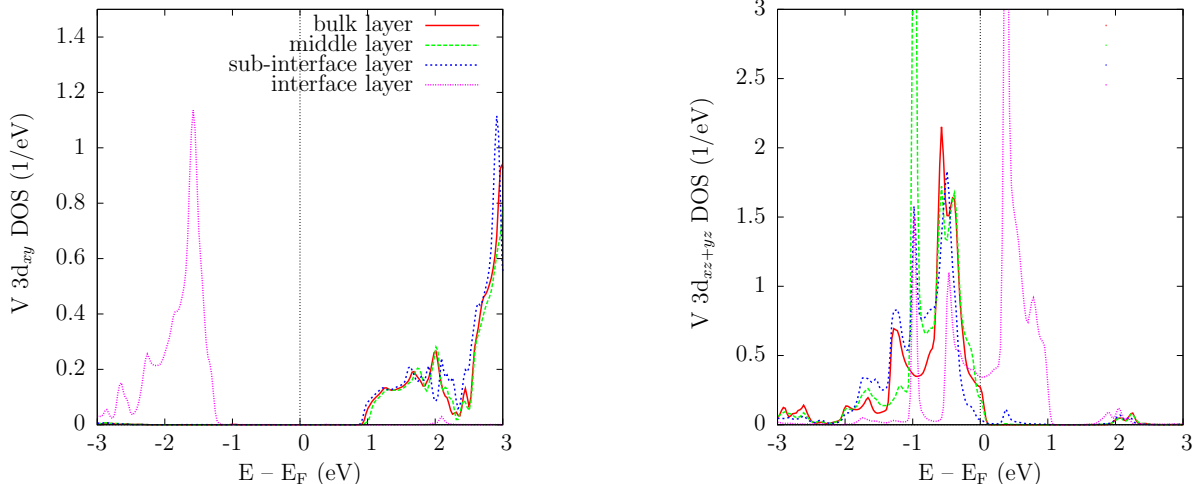


FIG. 3: (Color online) Density of states projected on the (left) $V 3d_{xy}$ and (right) $V 3d_{xz,yz}$ orbitals in the $m = 6$ superlattice. The inversion layer is denoted as bulk layer. The labeling of the layers is shown in Fig. 2.

tive of the odd and even superlattices, respectively. The lattice constants are $a = 3.88 \text{ \AA}$ and $c = (m + 1)3.95 \text{ \AA}$.

As observed experimentally, the c/a ratio in the superlattice deviates from the bulk ratio of LaVO_3 .¹⁴ In bulk LaVO_3 it is smaller than 1, $c/a = 0.98$,³⁰ but the strain exerted by the SrVO_3 layers distorts the LaVO_3 sublayers in the superlattice. In case of the odd superlattice, six VO_2 layers lie in between the SrO layers and the LaO forms the inversion layer, while in the even superlattice with its seven VO_2 layers, the central VO_2 layer is the inversion layer (see Figure 2).

In a first step, we neglect the antiferromagnetic order in the ab -plane and restrict ourselves to a 1×1 supercell in the ab -plane. In c -direction, ferromagnetic alignment is proposed, as expected for C-type spin order. It turns out in a second step that when taking into account also the magnetic ordering in the ab -plane by a 2×2 supercell the results concerning the interface electronic structure do not depend on the ordering in the ab -plane.

A. Superlattice $m = 6$

Let us start our investigations with the $m = 6$ superlattice and first focus on the orbital occupancy reconstruction at the interface. Deep in the LaVO_3 region a V^{3+} valency is realized, with the $3d_{xz}$ and $3d_{yz}$ orbitals occupied and the $V 3d_{xy}$ orbitals empty, as revealed by Fig. 3. On the contrary, for the interface layers (the two VO_2 layers adjacent to the SrO layer) the $V 3d_{xy}$ orbital is occupied and the $V 3d_{xz,yz}$ orbitals are partially occupied, see Fig. 3, together with a small admixture of the e_g orbitals. This results in a smaller valency of the V ions, which shows that they mostly retain the oxidation state of the respective bulk material. This provides us with a first indication that the doping of LaVO_3 is geometrically

confined.

This statement is further confirmed by the band structure shown in Fig. 4. It exhibits four interface-based bands crossing the Fermi energy, two of them giving rise to fairly symmetrical Fermi surfaces (in the $k_x k_y$ -plane) centered around the Γ point. These bands are characterized by rather large Fermi velocities. In addi-

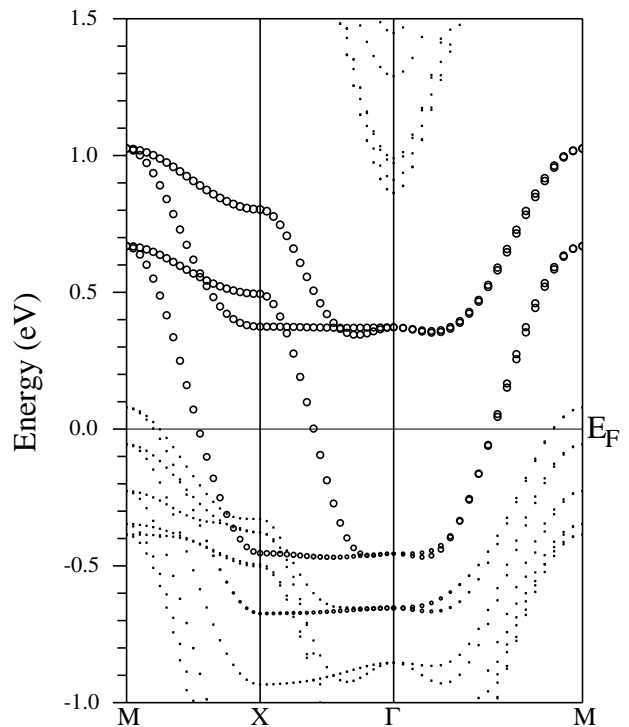


FIG. 4: Band structure of the $m = 6$ superlattice with non-magnetic interfaces. The interface $V 3d_{xz} + 3d_{yz}$ orbitals are highlighted.

tion, small hole pockets centered around the M-point are found. They are characterized by clearly smaller Fermi velocities and are due to bulk states. Therefore, the fast charge carriers are mostly confined to the interface layers, though in states also containing a small admixture from the sub-interface layer. Additional features of the band structure point to an interesting two-dimensional character of the bands crossing the Fermi energy. Principally constituted by d_{xz} (d_{yz}) orbitals which disperse along the Γ -X (Γ -Y) direction, they unexpectedly show considerable dispersion along X-M (Y-M), pointing to an admixture of other orbitals to the d_{xz} (d_{yz}) orbitals. Also, the dispersion around the Γ point is rather flat and not cosine-like as one would be expected for pure d_{xz}/d_{yz} bands.

A partial occupation of the d_{xz} and d_{yz} orbitals establishes the prerequisite of an orbitally ordered state. However, this is neither observed in our calculations nor in the experiments, where it was shown that these systems resemble rather good metals at low temperature.¹⁴ An explanation for this behavior may be found in the observed structure relaxations, where the most important ones are summarized in table I. In the interface layers the V (O) ions move towards (off) the SrO layers, resulting in a sizeable buckling of the interface layers with an amplitude close to 0.11 Å. The first LaO layers move quite homogeneously towards the SrO layer, with a buckling amplitude smaller than 0.01 Å, while the buckling amplitude of the sub-interface VO_2 layer is close to 0.04 Å.

As a result, the bond lengths are strongly reduced between the V ions in the interface VO_2 layers and the O ions in the SrO layer, becoming smaller than $a/2$, i.e., the distance of the V ion to the O ions in the xy -plane of the sample positioned at $a/2$ is larger than that to the O ion in the z -direction. Consequently, the non-degenerate V energy level ε_{xy} lies below the $\varepsilon_{xz,yz}$ levels in the interface layer, leading to an enhancement of the dispersion in those layers. On the other hand, the enlarged bond length between the interface layer and the adjacent LaO layer suppresses the orbital overlap in the z -direction and favors therefore an electronic decoupling of the interface VO_2 layer with respect to the other VO_2 layers, as shown in Figure 5. The same tendency of the buckling can still be seen in the sub-interface layer, but

TABLE I: Displacements (in Å) off SrO layers of the V and O atoms in the interface and middle/sub-interface layers for the heterostructures with $m = 5$ and $m = 6$. In the first LaO layers for $m = 5$ ($m = 6$) the motion towards the SrO layer of the La ions amounts to 0.118 Å (0.093 Å), and that of the O ions to 0.116 Å (0.010 Å).

	$m = 5$		$m = 6$	
	V	O	V	O
Interface layer	-0.022	0.096	-0.038	0.076
Middle/sub-interface layer	-0.0046	0.0029	-0.0027	0.0159

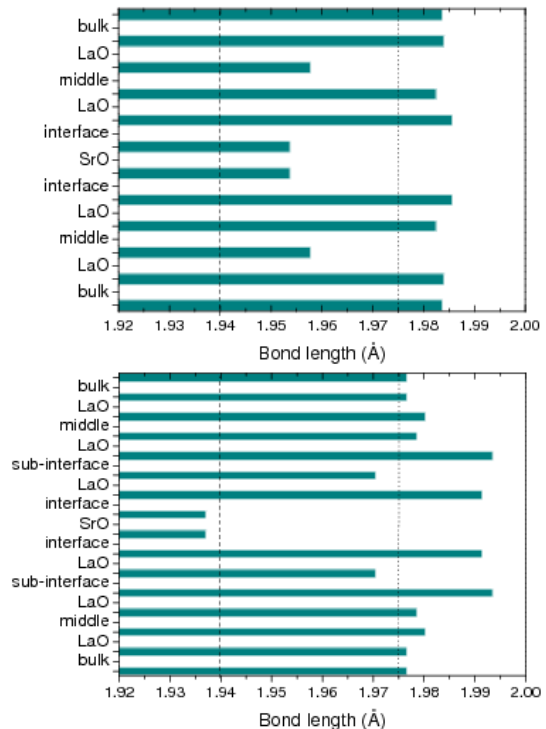


FIG. 5: (Color online) V-O and O-V bond lengths along the z -direction for $m = 5$ (top) and $m = 6$ (bottom). The vertical dashed line indicates $a/2$.

with a much smaller amplitude. The O-V bond length in this case is near to $c/2$ as for the other VO_2 layers. Thus, the larger distance between the V ions and the surrounding O atoms is to be found along the z -direction, inducing the bulk orbital occupancy and, hence, an orbitally ordered insulating state like in the bulk.

Thus, the calculated band structure accounts for a two-dimensional metallic state, but it cannot account for the experimentally observed ferromagnetism. In a Stoner picture this would be understood as the result of a rather small DOS at the Fermi energy. Therefore, should this system be ferromagnetic then ferromagnetism would likely be caused by further correlation effects, as taken into account in calculations of multi-orbital Hubbard models.^{18,19} Moreover, we have verified that the above electronic structure is stable against the employed U value and lattice relaxation, as is the establishment of an ultrathin two-dimensional electron gas.

B. Superlattice $m = 5$

The $m = 5$ superlattice hosts different physics. Again, lattice relaxation plays an important role. The obtained buckling of the interface layers is summarized in Table I. The interface VO_2 layer shows a buckling with the same displacement directions as for $m = 6$ (the V ions move towards the SrO layer and the O ions towards the LaO

layer) but the amplitude is smaller. Notably, as shown in Fig. 5, while for the $m = 6$ case the distance between the V ion in the interface layer and the O ion in the SrO layer becomes smaller than $a/2$, inducing the inversion of the orbital occupancy, in the $m = 5$ case the bond lengths stay larger than $a/2$ in all the VO_2 layers. The smaller amplitude of the buckling therefore does not induce an inversion of the orbital occupation and the confinement of the charge carriers is clearly less effective than in the even case. Furthermore, the reduction of the bond lengths reaches further into the LaVO_3 layer, where the bond length of the V ion with the second LaO layer counted from the SrO layer is still strongly reduced. In comparison, in the $m = 6$ case the same bond length is larger than $c/2$.

The change of the structural relaxation is visible in the resulting layer-projected densities of states in Fig. 6. They consist of the spin-majority density of states, as no sizeable contribution from the spin-minority bands is obtained. All layers are clearly off stoichiometry and all V ions are in a mixed valency state, yet closer to the 3+ valency in the bulk layers than in the interface layers. Moreover, all V $3d$ electrons occupy the $3d_{xz}$ and $3d_{yz}$ orbitals, while all $3d_{xy}$ orbitals are empty, in contrast to the $m = 6$ superlattice.

The band structure of the $m = 5$ superlattice is shown in Fig. 7. As there are no spin-minority bands close to the Fermi level, only spin-majority bands are shown. There are two narrow bands formed by the interface V $3d_{xz,yz}$ orbitals around the Fermi level. The four next lower lying bands are due to the middle and bulk layers with a larger band width. The bands at the Fermi level are separated by a band gap of about 1 eV (measured at

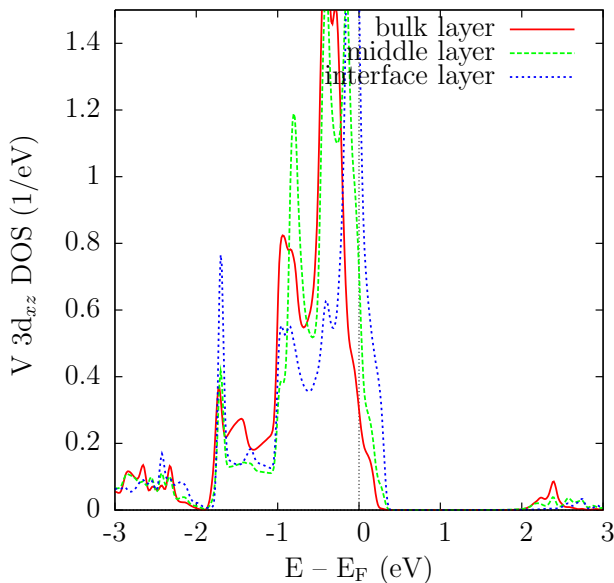


FIG. 6: (Color online) Spin-majority density of states projected on the V $3d_{xz}$ orbital. The labeling of the layers is shown in Fig. 2.

the Γ point) from the parabolic bands of the bulk states. In addition, the bands with the largest Fermi velocities mostly trace back to the middle layer V $3d_{xz,yz}$ orbitals, with some admixtures of the bulk and interface layers. Therefore, transport is no longer confined to the interface layers but there is a distinct modulation associated to it. There are fast charge carriers mostly confined to the next-to-interface layer, with a small admixture of their two neighbors, and slow charge carriers mostly confined to the interface layer.

Narrow d bands with high DOS at the Fermi level often explain ferromagnetism in the $3d$ transition metal oxides. Here the high DOS follows from the slow charge carriers that are confined to the interface layers. We therefore have performed calculations for 2×2 supercells in the ab -plane and find that the ground state shows a ferromagnetic alignment of the spins within the interface layer, whereas they are aligned antiferromagnetically in the other layers.

IV. CONCLUSION AND OUTLOOK

Our calculations show that the doping resulting from the charge carriers donated by the SrO layers in $(\text{LaVO}_3)_m/\text{SrVO}_3$ superlattices leads to rich physics built on fast and slow charge carriers together with lattice relaxation. For both types of superlattices the lattice relaxation plays an important role, demonstrated by the

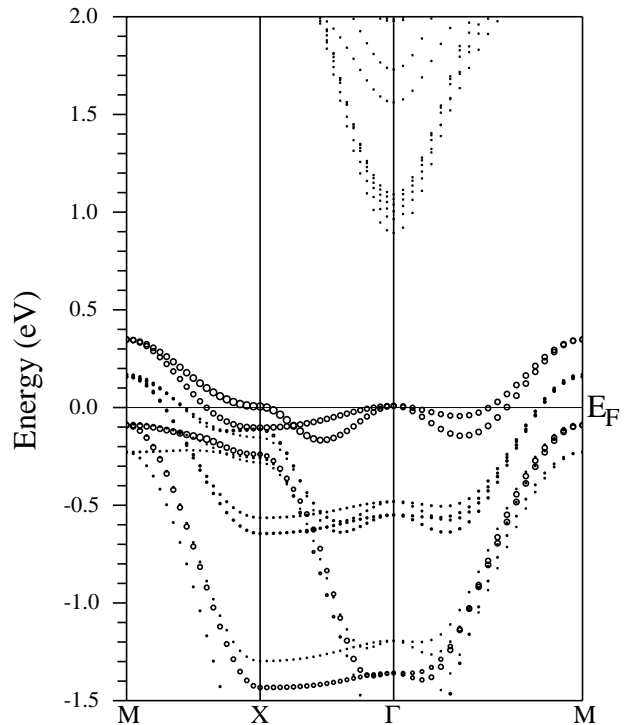


FIG. 7: Band structure of the $m = 5$ superlattice with ferromagnetically polarized interfaces. The interface V $3d_{xz} + 3d_{yz}$ orbitals are highlighted.

obtained buckling of the VO_2 interface layers and alteration of short and long V-O bond lengths along the c -axis. Although the buckling of the interface VO_2 layers is qualitatively the same in the two studied cases, the critical difference in the amplitude leads to two different band structures. In the odd $m = 5$ case, slow charge carriers are mostly confined to the interface layers in which they order ferromagnetically. The confinement of the fast charge carriers is less effective and their distribution peaks in the middle layers. For even superlattices the relaxation confines the fast charge carriers to largely decoupled interface layers in which they form an ultrathin two-dimensional electron gas. No magnetic order is found and the distribution of slow charge carriers peaks in the sub-interface layers. Therefore, coming back to our original question, it seems unlikely that the geometric confinement of the charge carriers alone is the origin of the experimentally observed ferromagnetic state. Instead, the fact that the even and odd superlattices show a different behavior points out the relevance of the number of unit cells of the LaVO_3 layers.

In our calculations we did not take into account the orthorhombic structure of LaVO_3 ,³⁰ generated by the octahedral tilts which were shown to be present in pure LaVO_3 thin films as well.³¹ The related unit cell is larger than the tetragonal cell used in the calculations, in particular along the tetragonal c -axis, where the out of phase rotation of the octahedra leads to a doubling of the unit cell, see Fig. 2. Therefore, in an even superlattice it is possible to establish the bulk structure including the octahedral rotations in the LaVO_3 layer. On the other hand, in the odd superlattice the thickness of the LaVO_3 layer corresponds to a half-integer number of the orthorhombic unit cell, so that the bulk structure (and therefore the bulk physics) of the LaVO_3 layer cannot be established. The compensation by the structure of the lack of the energetically favorable out of phase rotation may lead to the small but critical differences of the lattice relaxations and therefore the orbital occupations between the even and odd case. The combination of the individual reactions of the structural, orbital, and

electronic degrees of freedom leads in the end to a ferromagnetic ground state in the odd superlattices.

Our calculations confirm therefore the experimentally observed magnetization oscillations,¹⁵ although in the experiment the even superlattices were found to show a higher magnetization than the odd ones. This difference can be explained by the fact that the thickness of the LaVO_3 in the experimental study is a nominal one, where the announced thickness does not take into account any intermixing of La and Sr during the growth. It was shown that the interface between the LaVO_3 and SrVO_3 layers is abrupt but exhibits steps of typically one perovskite unit cell.³² The steps lead to the presence of Sr atoms in the first LaO layer next to the SrO layer. Taking into account the growth direction, it can be argued that the thickness of the pure LaVO_3 layer will thus be one unit cell less than the nominal one, resulting in an inversion of the nominally odd and nominally even superlattices.

In conclusion, two scenarios for the even and odd superlattice have been found. In both cases, the d_{xz} and d_{yz} orbitals form bands crossing the Fermi level. In the even superlattice, the orbital occupancy changes from the interface to the bulk layers, while we find an homogeneous orbital occupation in the odd superlattice. The room temperature magnetism is related to the incomplete formation of the orthorhombic unit cell of LaVO_3 in odd superlattices. A next step could be a comparison of theoretical and experimental macroscopic transport properties of the confined fast charge carriers.

Acknowledgments

We thank S. Nazir for valuable discussions. Financial support by the German Research foundation within TRR 80 (CS) and by the ANR through GeCoDo-ANR-2011-JS0800101 (UL and RF) is acknowledged. UL and RF gratefully acknowledge the Région Basse-Normandie and the Ministère de la Recherche for financial support.

-
- ¹ A. P. Malozemoff, J. Mannhart, and D. Scalapino, *Phys. Today* **58**, 41 (2005).
- ² J. G. Bednorz and K. A. Müller, *Z. Physik B* **64**, 189 (1986); B. Raveau, C. Michel, M. Hervieu, and D. Groult, *Crystal Chemistry of High- T_c Superconducting Copper Oxides*, Springer Series in Material Science **15**, Springer-Verlag Berlin, Heidelberg, New York (1991).
- ³ H. Kawazoe, H. Yasakuwa, H. Hyodo, M. Kurota, H. Yanagi, and H. Hosono, *Nature* **389**, 939 (1997).
- ⁴ L. Li, C. Richter, S. Paetel, T. Kopp, J. Mannhart, and R. C. Ashoori, *Science* **332**, 825 (2011).
- ⁵ I. Terasaki, Y. Sasago, and K. Uchinokura, *Phys. Rev. B* **56** 12 685 (R) (1997); A. Maignan, V. Eyert, C. Martin, S. Kremer, R. Frésard, and D. Pelloquin, *Phys. Rev. B* **80**, 115103 (2009).
- ⁶ A. Ohtomo and H. Y. Wang, *Nature (London)* **427**, 423 (2004).
- ⁷ S. Thiel, G. Hammerl, A. Schmehl, C. W. Schneider, and J. Mannhart, *Science* **313**, 1942 (2006).
- ⁸ M. Ben Shalom, A. Ron, A. Palevski, and Y. Dagan, *Phys. Rev. Lett.* **105**, 206401 (2010).
- ⁹ M. Kim, C. Bell, Y. Kozuka, M. Kurita, Y. Hikita, and H. Y. Hwang *Phys. Rev. Lett.* **107**, 106801 (2011).
- ¹⁰ H. W. Jang, D. A. Felker, C. W. Bark, Y. Wang, M. K. Niranjan, et al, *Science* **331**, 886 (2011).
- ¹¹ A. F. Santander-Syro et al., *Nature (London)* **469**, 189 (2011).
- ¹² N. Reyren et al., *Science* **317**, 1196 (2007).
- ¹³ L. Li, C. Richter, J. Mannhart, and R. C. Ashoori, *Nature Phys.* **7**, 762 (2011).

- ¹⁴ A. David, R. Frésard, Ph. Boullay, W. Prellier, U. Lüders, and P.-E. Janolin, *Appl. Phys. Lett.* **98**, 212103 (2011).
- ¹⁵ U. Lüders, W. C. Sheets, A. David, W. Prellier, and R. Frésard, *Phys. Rev. B* **80**, 241102R (2009).
- ¹⁶ F. Inaba, T. Arima, T. Ishikawa, T. Katsufuji, and Y. Tokura, *Phys. Rev. B* **52**, R2221 (1995).
- ¹⁷ S. Miyasaka, T. Okuda, and Y. Tokura, *Phys. Rev. Lett.* **85**, 5388 (2000).
- ¹⁸ C.-K. Chan, P. Werner, and A. J. Millis, *Phys. Rev. B* **80**, 235114 (2009).
- ¹⁹ R. Frésard and M. Lambole, *J. Low Temp. Phys.* **126**, 1091 (2002).
- ²⁰ G. Jackeli and G. Khaliullin, *Phys. Rev. Lett.* **101**, 216804 (2008).
- ²¹ V. Pardo and W. E. Pickett, *Phys. Rev. B* **81**, 245117 (2010).
- ²² H. Weng and K. Terakura, *Phys. Rev. B* **82**, 115105 (2010).
- ²³ G. Khaliullin, P. Horsch, and A. M. Oleś, *Phys. Rev. Lett.* **86**, 3879 (2001); *Phys. Rev. B* **70**, 195103 (2004).
- ²⁴ J. Fujioka, T. Yasue, S. Miyasaka, Y. Yamasaki, T. Arima, H. Sagayama, T. Inami, K. Ishii, and Y. Tokura, *Phys. Rev. B* **82**, 144425 (2010).
- ²⁵ V. I. Anisimov, F. Aryasetiawan, and A. I. Lichtenstein, *J. Phys.: Condens. Matter* **9**, 767 (1997).
- ²⁶ U. Schwingenschlögl and C. Schuster, *Phys. Rev. Lett.* **99**, 237206 (2007).
- ²⁷ U. Schwingenschlögl, C. Schuster, and R. Frésard, *EPL* **88**, 67008 (2009).
- ²⁸ P. Blaha, K. Schwarz, G. Madsen, D. Kvasnicka, and J. Luitz, *Wien2k: An augmented plane wave + local orbitals program for calculating crystal properties*, Vienna University of Technology (2001).
- ²⁹ I. H. Inoue, O. Goto, H. Makino, N. E. Hussey, and M. Ishikawa, *Phys. Rev. B* **58**, 4372 (1998).
- ³⁰ P. Bordet, C. Chaillout, M. Marezio, Q. Huang, A. Santoro, S. W. Cheong, H. Takagi, C. S. Oglesby, and B. Batlogg, *J. Sol. State Chem.* **106**, 253 (1993).
- ³¹ H. Rotella, U. Lüders, P.-E. Janolin, V. H. Dao, D. Chateigner, R. Feyerherm, E. Dudzik, and W. Prellier, *Phys. Rev. B* **85**, 184101 (2012).
- ³² P. Boullay, A. David, W. C. Sheets, U. Lüders, W. Prellier, H. Tan, J. Verbeeck, G. Van Tendeloo, C. Gatel, G. Vincze, and Z. Radi, *Phys. Rev. B* **83**, 125403 (2011).